Published in final edited form as:

Neuroscience. 2016 August 04; 329: 66–73. doi:10.1016/j.neuroscience.2016.04.054.

LOSS OF ESTROGEN-RELATED RECEPTOR ALPHA DISRUPTS VENTRAL-STRIATAL SYNAPTIC FUNCTION IN FEMALE MICE

HÉCTOR DE JESÚS-CORTÉS[a,†], **YUAN LU**[a], **RACHEL M. ANDERSON**[b], **MICHAEL Z. KHAN**[a], **VARUN NATH**[a], **LATISHA MCDANIEL**[a], **MICHAEL LUTTER**[a], **JASON J. RADLEY**[b], **ANDREW A. PIEPER**[a,c,d], **HUXING CUI**[a,*]

[a]Department of Psychiatry, University of Iowa, Carver College of Medicine, Iowa City, IA, USA

[b]Department of Psychology, University of Iowa, Carver College of Medicine, Iowa City, IA, USA

[c]Department of Neurology, University of Iowa, Carver College of Medicine, Iowa City, IA, USA

[d]Free Radical & Radiation Biology Program, Department of Radiation Oncology Holden Comprehensive Cancer Center, University of Iowa, Carver College of Medicine, Iowa City, IA, USA

Abstract

Eating disorders (EDs), including anorexia nervosa, bulimia nervosa and binge-ED, are mental illnesses characterized by high morbidity and mortality. While several studies have identified neural deficits in patients with EDs, the cellular and molecular basis of the underlying dysfunction has remained poorly understood. We previously identified a rare missense mutation in the transcription factor estrogen-related receptor alpha (ESRRA) associated with development of EDs. Because ventral-striatal signaling is related to the reward and motivation circuitry thought to underlie EDs, we performed functional and structural analysis of ventral-striatal synapses in Esrra-null mice. Esrra-null female, but not male, mice exhibit altered miniature excitatory postsynaptic currents on medium spiny neurons (MSNs) in the ventral striatum, including increased frequency, increased amplitude, and decreased paired pulse ratio. These electrophysiological measures are associated with structural and molecular changes in synapses of MSNs in the ventral striatum, including fewer pre-synaptic glutamatergic vesicles and enhanced GluR1 function. Neuronal Esrra is thus required for maintaining normal synaptic function in the ventral striatum, which may offer mechanistic insights into the behavioral deficits observed in Esrra-null mice.

Keywords

estrogen-related receptor alpha; eating disorder; synaptic transmission; ventral striatum; miniature excitatory postsynaptic currents; sexual dimorphism

*Corresponding author. Present address: Department of Pharmacology, Center for Hypertension Research, Fraternal Order of Eagles Diabetes Research Center, University of Iowa, Carver College of Medicine, 51 Newton Road, 2-372 BSB, Iowa City, IA 52242, USA. Tel: +1-319-335-6954; fax: +1-319-335-8930. Huxing-Cui@uiowa.edu (H. Cui).

†Present address: The Picower Institute for Learning and Memory, Massachusetts Institute of Technology, Cambridge, MA 02139, USA.

INTRODUCTION

Eating disorders (EDs) are thought to develop as a result of environmental stress superimposed upon genetic vulnerability (Kaye et al., 2013). Worldwide prevalence of EDs is highest in women, especially in adolescent girls, with a male to female ratio ranging from 1:3 to 1:10, depending on the population studied (Smink et al., 2012). Several studies utilizing functional imaging in ED patients have identified deficits in neural activation in response to a variety of tasks, indicating that neuronal dysfunction may contribute to the development of EDs (Lutter et al., 2015). However, the cellular and molecular basis of these deficits has remained poorly understood, in part due to the lack of rigorous rodent models of EDs. To facilitate the genetic and neurobiologic understanding of EDs, we performed a family-based genetic analysis to identify rare mutations that increase the risk of developing an ED (Cui et al., 2013). Specifically, we identified an arginine to glutamine missense mutation in the transcription factor estrogen-related receptor alpha ($ESRRA^{R188Q}$), which reduces transcriptional activity of ESRRA *in vitro* (Cui et al., 2013). Behavioral analysis of Esrra-null mice revealed several behavioral deficits relevant to EDs, including decreased operant responding for high-fat diet after overnight fasting, compulsive grooming, and social subordination (Cui et al., 2015). Furthermore, female mice exhibit more pronounced behavioral deficits than male mice, suggesting that estrogen signaling may impinge upon Esrra activity in some manner.

Research in other fields of study has highlighted a complicated relationship between Esrra and estrogen receptor activity. Unlike estrogen receptor, Esrra does not require estrogen binding for transcriptional activity, and instead utilizes peroxisome proliferator-activated receptor gamma coactivator 1-alpha (PGC-1α) as an obligate transcriptional co-activator (Giguere, 2002). However, ESRRA and estrogen receptor alpha do bind to related DNA elements. For example, ESRRA binds as a monomer to the consensus extended half-site TnAAGGTCA, estrogen receptor alpha binds as a dimer to the inverted repeat sequence of AGGTCA, and ESRRA can induce expression of genes with an estrogen response element *in vitro* (Giguere, 2002). Taken together, these observations suggest possible crosstalk at the level of transcriptional regulation. While an initial study found that ESRRA modulated estrogen receptor alpha-mediated induction of the lactoferrin gene (Yang et al., 1996), the degree to which estrogen receptor alpha and ESRRA share common targets on a genome-wide scale is unclear (Stein et al., 2008).

In order to better understand the role of Esrra in the brain, we have now executed rigorous functional and structural analysis of glutamatergic synapses on medium spiny neurons (MSNs) in the ventral striatum of female and male Esrra-null mice. We find that Esrra-null female, but not male, mice exhibit electrophysiological and structural changes in glutamatergic synapses on ventral striatal MSNs. These findings offer new insights in the sex-specific function of Esrra in the brain.

EXPERIMENTAL PROCEDURES

Animals

Esrra-null mice were generated as previously reported (Luo et al., 2003) and backcrossed >5 generations onto C57BL/6 (Jackson Laboratory, Bar Harbor, ME, USA). All animal procedures were performed in accordance with University of Iowa Institutional Animal Care and Use Committee guidelines. All mice used in this study were handled in accordance with the Guide for the Care and Use of Laboratory Animals as adopted by the U.S. National Institutes of Health, and specific protocols were approved by the Institutional Animal Care and Use Committee.

Electrophysiology

Nucleus accumbens (NAc) MSNs were morphologically identified by DIC microscopy (Nikon Eclipse E600FN). As previously reported (Kreple et al., 2014), whole-neuron recordings were sampled at 10 kHz using an Axopatch 200B amplifier (Axon Instruments, Foster City, CA, USA). Data were digitized by DigiData 1322A and analyzed with ClampFit 10 (Axon software, Sunnyvale CA, USA). Recording pipettes were pulled with standard borosilicate capillaries by a Flaming-Brown electrode puller (P-97, Sutter Instruments Co., Novato, CA, USA), and were filled with patch solution (in mM: 125 K Gluconate, 20 KCl, 10 NaCl, 2 Mg-ATP, 0.3 Na-GTP, 2.5 QX314, 10 HEPES, 0.2 EGTA, pH 7.3 adjusted with KOH). Resistance ranged between 3 and 6 MΩ, and excitatory postsynaptic currents (EPSCs) were evoked with a bipolar tungsten electrode. Paired pulse facilitation (PPF) was measured at an inter-stimulus interval of 50 ms. AMPAR-mediated miniature EPSCs (mEPSCs) were recorded with a holding potential of–70 mV in the presence of 1 μM tetrodotoxin (TTX, Tocris, Avonmouth, Bristol, UK) to block voltage-gated Na+ channels and 100 μM picrotoxin to block GABAA receptors. We used ClampFit 10 (Axon software) to analyze mEPSCs. Access resistance criteria was <30 MΩ and mEPSC detection threshold was 3 pA.

Dendritic spine morphologic analysis

Dendritic spine density and morphology was measured as previously described (Radley et al., 2008; Anderson et al., 2014). Drug-naive sixteen- week-old wild-type (WT) and Esrra-null mice were anesthetized using ketamine/xylazine and transcardially perfused with 1% paraformaldehyde (vol/vol) in phosphate-buffered saline (PBS), followed by perfusion with 4% paraformaldehyde/0.125% glutaraldehyde (vol/vol) in PBS. MSNs in 250-μm-thick coronal sections containing the NAc core were identified by morphology and injected with 5% Lucifer yellow (vol/ vol, Invitrogen, Waltham, MA, USA) via micropipette iontophoresis (1–2-μm inner diameter) under 5 min of direct current of 1–6 nA. Sections were mounted on glass slides and coverslipped in VectaShield (Vector Laboratories, Burlingame, CA, USA). Dendritic segments were imaged with a Leica SP5 confocal microscope with a 100×, 1.4 N. A. oil-immersion objective, using voxel dimensions of 0.1 × 0.1 × 0.1 μm^3. Non-overlapping, completely filled dendritic segments from the NAc core were randomly selected between 50 and 150 μm from the soma for high-resolution imaging. Images were deconvolved with AutoDeblur (Media Cybernetics, Rockville, MD, USA), and semi-automated three-dimensional analyses were conducted with NeuronStudio on spine

density and morphometric features (head/neck diameter, length) (http://research.mssm.edu/cnic/tools-ns.html) (Rodriguez et al., 2006). Thin or mushroom spines were designated as having head-to-neck diameter ratio >1.1:1. Spines with head diameter >0.35 μm were classified as mushroom, or otherwise classified as thin. Spines with head-to-neck diameter ratios <1.1:1 were also classified as thin if the ratio of spine length-to-neck diameter was greater than 2.5. Otherwise, they were classified as stubby. Filopodial spines, having a long and thin shape with no enlargement at the distal tip, were seldom observed and classified herein as thin. An average of five neurons was imaged per mouse, and 2–4 dendritic segments were imaged per neuron. 10,106 dendritic spines were analyzed in total (4626 spines in WT mice, 5480 spines in Esrra-null mice).

Transmission electron microscopy (TEM) and quantification of synaptic vesicles

Brain sections from 16- week-old female and male WT and Esrra-null mice were prepared for TEM by standard methods. Anesthetized mice were transcardially perfused with Karnovsky's fixative solution (2% formaldehyde, 2.5% glutaraldehyde, 0.2 M sodium cacodylate buffer, 1 mM $CaCl_2$, 2 mM $MgCl_2$, and 42.8 mM NaCl, pH 7.4). Harvested brains were incubated in Karnovsky's fixative solution overnight at 4 °C. Whole brains were cut in the coronal plane (200 μm) using a vibratome (Leica 1500, Buffalo Grove, IL, USA). Sections that contained the striatum were selected, washed with 0.1 M sodium cacodylate buffer and then post fixed with 1% osmium fixative for 1 h. After washing in 0.1 M sodium cacodylate buffer, sections were dehydrated in a series of ethanol (50%, 75%, 95% and 100% ethanol) followed by embedding in EPON resin overnight at 65 °C. Toluidine blue staining was used to select the ventral striatum using semithin sections (1 μm) cut with an ultramicrotome (Leica UC6). Pictures were taken using an upright microscope (Zeiss Axio Imager.M2) with a color camera (AxioCam ICc5), and ventral striatum was outlined for further processing. For TEM, ultrathin sections (60 nm) adjacent to semithin sections were cut with an ultramicrotome, loaded onto a Formvar 200-mesh Ni grid, and counterstained with uranyl acetate and lead citrate. Specimens were examined using a JEOL JEM 1230 electron microscope with a Gatan UltraScan 1000 2 k × 2 k CCD camera. Fifteen-20 images were captured at random across each section.

Two blinded experimenters analyzed all images. In each image, terminal bulbs to be quantified were selected based on high visible postsynaptic density. Each selected terminal bulb was then traced and measured for area using ImageJ Polygon Selection (ImageJ, NIH). Individual vesicles within the bulb were counted manually using the ImageJ Cell Counter Tool. Vesicle density was calculated using the total number of vesicles counted/area of the terminal button. In total, we selected three sections per group and the number of synapses (S) and images (I) we counted are as follows: three WT-females: S = 66, I = 54, four Esrra-null-females: S = 162, I = 117, four WT-males: S = 111, I = 82, five Esrra-null-males: S = 170, I = 132.

Western blot (WB)

Ventral striatum from sixteen- week-old experimentation-naïve WT and Esrra-null mice was collected and processed for WB as previously reported (Cui and Lutter, 2013). Fresh tissue was immediately frozen in liquid nitrogen and stored at –80 °C until use.

Small pieces of frozen tissue were homogenized in cold radioimmunoprecipitation assay buffer (#89901; Thermo Scientific, Waltham, MA, USA) containing cocktails of proteinase inhibitors (11836170001; Roche Diagnostics, Indianapolis, IN, USA) and phosphatase inhibitors (04906845001; Roche Diagnostics), and retained on ice for 30 min. Samples were then centrifuged (13,000 rpm) at 4 °C for 20 min, and the supernatant was taken as total protein extraction. Protein concentration was determined by BCA protein assay method (#23228; Thermo Scientific), and 20 μg of protein were separated by sodium dodecyl sulfate–polyacrylamide gel electrophoresis (SDS–PAGE) gel followed by transfer onto a polyvinylidene fluoride membrane. Primary antibodies were used as follows: anti-phospho- GluR1 Ser831antibody (04–823, 1:5000, Millipore, Billerica, MA, USA), antiphospho-GluR1 Ser845 antibody (AB5849, 1:5000, Millipore) and anti-GluR1 antibody (04–855, 1:1000, Millipore), anti-beta-actin antibody (#4970, Cell Signaling, Danvers, MA, USA). Membranes were then incubated with horseradish peroxidase–conjugated secondary antibody (Jackson ImmunoResearch, West Grove, PA, USA), and signals were detected by chemiluminescence. Signal intensity was measured and analyzed by a BioSpectrum 810 Imaging System (UVP, Upland, CA, USA). For each experiment, signal intensity of targeted phosphorylated proteins was normalized to beta-tubulin or total GluR1 signal intensity and then compared between groups.

Data analysis and figure preparation

For all experiments, data were first analyzed for normality using a Shapiro–Wilk test. Genotype and sex independent variables were individually analyzed for normality and skewness and kurtosis are reported in results. If the data were normally distributed, we used a parametric independent-samples t test or a two-way analysis of variance (ANOVA). For data that were not normally distributed, we used a non-parametric independent-samples Mann–Whitney U test for data that only had two groups, or Kruskal–Wallis H test for data that contained multiple groups (as specified in figure legends). A value of $p < 0.05$ was considered to be statistically significant, and all analyses were performed using SPSS version 19 (SPSS Inc, Chicago, IL, USA). Graphs were constructed in GraphPad Prism version 6.0 for Mac (San Diego, CA, USA). Final figures were assembled using Adobe Illustrator CS5 version 15.1.0. No image manipulation was applied to any figure panel other than size changes and color.

RESULTS

Synaptic transmission is altered in female, but not male, Esrra-null mice

Because Esrra-null mice display behavioral deficits relevant to EDs (Cui et al., 2013), we were interested in understanding the cellular and molecular basis of this dysfunction. We first focused on basal synaptic transmission, which is frequently disrupted in other neuropsychiatric disorders, such as autism and schizophrenia (Glantz and Lewis, 2000; Hutsler and Zhang, 2010; Penzes et al., 2011). To understand the role of Esrra in basal synaptic transmission, we assessed glutamatergic transmission onto MSNs in the NAc core, a region of the ventral striatum often identified as having aberrant function in human neuroimaging studies of patients with EDs (Wagner et al., 2008; Zastrow et al., 2009; Keating et al., 2012; Wierenga et al., 2015), from female and male WT and Esrra-null

littermates. We recorded mEPSCs to assess changes in pre- and post-synaptic function. The age of mice ranged from 16 to 20 weeks, corresponding with the time frame during which behavioral deficits were prominently observed (Cui et al., 2015). We first determined amplitude of mEPSCs and observed non-normal distribution for both females and males, with skewness of 1.18 (SE = .361), and 1.48 (SE = .357) and kurtosis of .909 (SE = .709), and 2.83 (SE = .702), respectively. We also observed non-normal distribution for both WT and Esrra-null mice, with skewness of 2.34 (SE = .361), and 1.41 (SE = .357), and kurtosis of 7.03 (SE = .709), and 2.82 (SE = .702), respectively. We therefore analyzed the data using a non-parametric Kruskal–Wallis *H* test, which revealed a significant difference between both sex and genotypes ($\chi^2(3) = 19.42$, $p < .001$, Fig. 1A, B). Analysis of individual groups showed a significant increase in peak amplitude of Esrra-null females compared to WT females ($\chi^2(1) = 4.57$, $p = .033$), but no genotype-specific difference in males ($\chi^2(1) = .344$, $p = .557$). Interestingly, however, increased peak amplitude in Esrra-null female mice was comparable to male WT and Esrra-null mice ($\chi^2(1) = 2.05$, $p = .152$), indicating that peak amplitude of mEPSCs in WT NAc core is lower in females than males ($\chi^2(1) = 9.22$, $p = .002$). We also analyzed the frequency of mEPSCs and observed that the data were normally distributed for both sex and genotype (Fig. 1C). Using two-way ANOVA with genotypes and sex as between factors revealed a main effect in both sex ($F(1, 83) = 5.06$, $p = .027$) and genotype ($F(1, 83) = 6.41$, $p = .013$). These main effects were not qualified by an interaction of sex and genotypes ($F(1, 83) = 2.86$, $p = .095$). Bonferroni post hoc analysis revealed a significant difference between WT and Esrra-null females ($p = .023$), and also between WT females and WT males ($p = .041$), in line with our measurements of peak amplitude. No significant differences were observed in Esrra-null females compared to WT males ($p > .999$). Lastly, we analyzed decay tau of mEPSCs (Fig. 1D) and observed a normal distribution. A two-way ANOVA revealed no significant differences in either sex ($F(1, 83) = .90$, $p = .344$) or genotype ($F(1, 83) = 2.21$, $p = .141$).

As an additional measure of changes in pre-synaptic function, we recorded paired evoked EPSCs and calculated paired-pulse ratio (PPR). Here, we observed that sex was non-normally distributed with female and male skewness of .956 (SE = .393) and 1.30 (SE = .393), respectively, and kurtosis of .377 (SE = .768) and 1.89 (SE = .768), respectively. We also observed that genotype was non-normally distributed with WT and Esrra-null mice, with skewness of .682 (SE = .393) and 1.90 (SE = .393), respectively, and kurtosis of -.110 (SE = .768) and 3.98 (SE = .768), respectively. Kruskal–Wallis *H* test revealed a significant difference between both sex and genotypes ($\chi^2(3) = 18.10$, $p < .001$, Fig. 1E). Analysis of individual groups showed a significant reduction in PPRs of Esrra-null females compared to WT females ($\chi^2(1) = 16.92$, $p < .001$), but no difference in males ($\chi^2(1) = .049$, $p = .825$). We observed no significant difference between WT females and WT males ($\chi^2(1) = 2.50$, $p = .114$), and a significant decrease in PPRs in Esrra-null females when compared to WT males ($\chi^2(1) = 8.66$, $p = .003$).

Synaptic vesicle pool density is reduced in female, but not male, Esrra-null mice

Increased mEPSC frequency is typically associated with either an increased probability of presynaptic vesicle release or an increased number of synapses (Wojcik and Brose, 2007; Sala and Segal, 2014). To test the first possibility, we conducted morphologic analyses of

synapses in the NAc core to identify morphologic correlates of the electrophysiological alterations observed in female Esrra-null mice. Specifically, we used TEM to quantify the amount of synaptic vesicles to calculate vesicle pool density (Fig. 2A, B). The data for both sex and genotype were normally distributed. Using a two-way ANOVA with genotypes and sex as between factors revealed a main effect in both sex ($F(1, 12) = 7.13$, $p = .020$) and genotype ($F(1, 12) = 9.54$, $p = .009$). These main effects were not qualified by an interaction of sex and genotypes ($F(1, 12) = 1.23$, $p = .289$). Bonferroni post hoc analysis revealed significant differences in WT females compared to Esrra-null females ($p = .032$), and in Esrra-null females compared to WT males ($p = .028$). No significant differences were observed between WT females and WT males ($p = .537$). This suggests that reduction of PPRs in female Esrra-null mice is associated with a decreased number of available vesicles to release.

To test the second possibility of altered synapse numbers, MSNs in the NAc core were loaded with Lucifer yellow fluorescent dye to facilitate imaging and analysis of dendritic spines (Fig. 2C). Here, we studied only female mice since no electrophysiological or structural changes were detected in male Esrra-null mice. We observed that the data were normally distributed, and no change in the number of spines of WT compared to Esrra-null female mice ($t(7) = .844$, $p = .427$). Analyses of spine subtype also revealed no change in spine density for each class (thin, $t(7) = .806$, $p = .447$, stubby, $t(7) = .351$, $p = .736$, mushroom, $t(7) = .087$, $p = .933$).

Increased GluR1 phosphorylation in female Esrra-null mice

Increased mEPSC amplitude can occur as a result of increases in site-specific phosphorylation of the GluR1 subunit of the AMPA receptor, which increase channel conductance (Ser^{831}) or peak open probability (Ser^{845}) (Wang et al., 2005). To test this possibility, fresh tissue punches of NAc were processed for WB. Only female mice were studied because synaptic dysfunction was only observed in female Esrra-null mice. First, we found that total GluR1 levels were not changed using beta actin as control (WT Mean = .28 and Esrra-null Mean = .21, unpaired Student's *t*-test $p = .08$). Next, we probed with antibodies for phosphorylated-GluR1 in separated membranes. Densitometric analysis revealed non-normal distribution for Esrra-null mice, with skewness of .863 (SE = 637) and kurtosis of .075 (SE = 1.23). A Mann–Whitney *U* test revealed significant increase in phosphorylation at both sites of Ser^{845} ($U = 5.0$, $p = .041$) and Ser^{831} ($U = 5.0$, $p = .041$) in female Esrra-null mice. These data suggest that there is an increase in GluR1 subunit AMPA receptor ion channel function (Fig. 3).

DISCUSSION

Establishing causality between transcriptional changes, synaptic plasticity, circuit function and behavior, such as food intake, is an important and challenging problem to address in both the fields of body weight homeostasis and neuropsychiatry. We have previously shown that loss of the transcription factor Esrra blunts behavioral responses to calorie restriction and increases behavioral compulsivity, with a more pronounced effect in female mice (Cui et al., 2015). However, the role of Esrra in neuronal function and how loss of Esrra affects

neuronal activity is unknown. In the present study we begin to fill in this knowledge gap by showing altered functioning of glutamatergic synapses, such as those in MSNs of the NAc core in Esrra-null female mice. This conclusion is supported by multiple functional and structural deficits observed in MSNs of the NAc core in Esrra-null mice, including increased frequency and amplitude of mEPSCs, decreased PPR and reduced presynaptic vesicle number. However the precise relationship between these deficits is unclear.

Increased frequency of mEPSCs can be due to either presynaptic (e.g. increased release probability) or postsynaptic (e.g. increased dendritic spine density) dysfunction. As spine density was not significantly different between WT and Esrra-null female mice, the increased frequency of mEPSCs may result from elevated release probability of pre-synaptic vesicles. Elevated release probability may also contribute to the observed decrease in PPR. PPR is dependent on many factors, including release probability after the first stimulation (P_{ves1}), release probability after the second stimulation (P_{ves2}), and size of the readily releasable vesicle pool (Hanse and Gustafsson, 2001). Increases in P_{ves1} have previously been associated with decreases in PPR, an effect that was more pronounced after depletion of pre-primed vesicles (Hanse and Gustafsson, 2001). While the current study was not designed to measure the size of the pre-primed vesicle pool, Esrra-null female mice did exhibit reduced overall number of vesicles consistent with this possibility. Another possibility is that the concentration of neurotransmitter per vesicle is higher in female Esrra-null mice, and therefore each vesicle is capable of releasing more glutamate into the synaptic cleft, thereby increasing synaptic transmission as has been previously observed (Wu et al., 2007). Future assessment of the pre-synaptic vesicle pools will be useful in deciphering these possibilities.

Increased amplitude of mEPSCs is typically associated with post-synaptic changes. Consistent with a possible post-synaptic mechanism, female Esrra-null mice displayed significantly increased phosphorylation of the GluR1 subunit of the AMPA receptor at the Ser^{831} and Ser^{845} residues. Previous studies have shown that phosphorylation at either site can potentiate AMPA receptor ion channel function (Derkach et al., 1999; Banke et al., 2000). However, function is augmented through different mechanisms, in that phosphorylation at Ser^{831} increases channel conductance (Derkach et al., 1999) while phosphorylation at Ser^{845} enhances AMPA current by increasing the open time probability of the channel (Roche et al., 1996). This is in accordance with our observed increase in both peak amplitude and frequency. As Esrra is expressed in low abundance in the ventral striatum (Cui et al., 2015), it is unclear whether the changes in mEPSC amplitude result from cell autonomous or non-autonomous mechanisms. Future studies using conditional deletion of Esrra are needed to clarify the mechanisms underlying increased mEPSC amplitude in female Esrra-null mice.

The mechanism of sex-specific differences that we observed is also of interest. Estrogen receptors have been localized to dendritic spines in glutamatergic neurons, and signaling through estrogen receptors increases the frequency of mEPSCs in hippocampal slices of female mice by signaling through estrogen receptor beta (Sala and Segal, 2014; Oberlander and Woolley, 2016). Previous research has suggested a potential interaction between Esrra and estrogen receptor signaling (Yang et al., 1996; Giguere, 2002; Stein et al., 2008),

indicating that it may be possible for Esrra activity to affect estrogen receptor beta signaling in neurons. Future work will focus on determining how Esrra-estrogen receptor interactions affect synaptic functioning and behavioral outputs in this system.

Several limitations of the current study are worth noting. First we did not record from MSNs in the ventral striatum in a cell-type specific manner, so we do not know if the electrophysiological changes that we observed were specific to dopamine 1 receptor+, dopamine 2 receptor+, or parvalbumin+ neurons. Likewise, we did not identify the source of the afferent glutamatergic neurons during recording. However the major glutamatergic inputs to the ventral striatum, including prefrontal cortex, ventral hippocampus, anterior cingulate cortex, motor/sensory cortex, and thalamus (Salgado and Kaplitt, 2015), all have high expression of Esrra (Cui et al., 2015) indicating that the majority of pre-synaptic inputs that we recorded from likely express Esrra.

In summary, we performed a structural and functional assessment of glutamatergic synapses on MSNs in the NAc of Esrra-null mice, and discovered sex-specific alterations in mEPSC frequency and amplitude, reduced PPR, and reduction in glutamatergic synaptic vesicles consistent with altered functional connectivity. Our findings thus provide new molecular insights into the role of Esrra in neuronal function, which may contribute to a better understanding of how loss of Esrra activity increases the risk of developing an ED.

Acknowledgments—

This material is based upon work supported by the National Science Foundation Graduate Research Fellowship #2012140236-02 (HDJ), the Dylan Tauber Researcher Award from the Brain and Behavior Foundation (ML), the Klarman Family Foundation Grants Program in Eating Disorder Research (ML), MH-095972 (JJR), and American Heart Association Scientist Developmental Grant #14SDG20140054 (HC), and unrestricted funds from the University of Iowa Carver College of Medicine (AAP). The authors are grateful to Jianqiang Shao for technical support of EM studies performed in the University of Iowa Central Microscopy Facility.

Abbreviations:

ANOVA	analysis of variance
EDs	eating disorders
EGTA	ethylene glycol tetraacetic acid)
EPSCs	excitatory postsynaptic currents
ESRRA	estrogen-related receptor alpha
HEPES	4-(2-hydroxyethyl)-1-piperazineethanesulfonic acid
mEPSCs	miniature excitatory postsynaptic currents
MSNs	medium spiny neurons
NAc	nucleus accumbens
PBS	phosphate-buffered saline

PRR	paired-pulse ratio
TEM	transmission electron microscopy
WB	Western blot
WT	wild-type

REFERENCES

Anderson RM, Birnie AK, Koblesky NK, Romig-Martin SA, Radley JJ (2014) Adrenocortical status predicts the degree of age-related deficits in prefrontal structural plasticity and working memory. J Neurosci 34:8387–8397. [PubMed: 24948795]

Banke TG, Bowie D, Lee H, Huganir RL, Schousboe A, Traynelis SF (2000) Control of GluR1 AMPA receptor function by cAMP-dependent protein kinase. J Neurosci 20:89–102. [PubMed: 10627585]

Cui H, Lutter M (2013) The expression of MC4Rs in D1R neurons regulates food intake and locomotor sensitization to cocaine. Genes Brain Behav 12:658–665. [PubMed: 23786641]

Cui H, Moore J, Ashimi SS, Mason BL, Drawbridge JN, Han S, Hing B, Matthews A, McAdams CJ, Darbro BW, Pieper AA, Waller DA, Xing C, Lutter M (2013) Eating disorder predisposition is associated with ESRRA and HDAC4 mutations. J Clin Invest 123:4706–4713. [PubMed: 24216484]

Cui H, Lu Y, Khan MZ, Anderson RM, McDaniel L, Wilson HE, Yin TC, Radley JJ, Pieper AA, Lutter M (2015) Behavioral disturbances in estrogen-related receptor alpha-null mice. Cell Rep 11:344–350. [PubMed: 25865889]

Derkach V, Barria A, Soderling TR (1999) Ca2+/calmodulin-kinase II enhances channel conductance of alpha-amino-3-hydroxy-5-methyl-4-isoxazolepropionate type glutamate receptors. Proc Natl Acad Sci USA 96:3269–3274. [PubMed: 10077673]

Giguere V (2002) To ERR in the estrogen pathway. Trends Endocrinol Metab 13:220–225. [PubMed: 12185669]

Glantz LA, Lewis DA (2000) Decreased dendritic spine density on prefrontal cortical pyramidal neurons in schizophrenia. Arch Gen Psychiatry 57:65–73. [PubMed: 10632234]

Hanse E, Gustafsson B (2001) Paired-pulse plasticity at the single release site level: an experimental and computational study. J Neurosci 21:8362–8369. [PubMed: 11606624]

Hutsler JJ, Zhang H (2010) Increased dendritic spine densities on cortical projection neurons in autism spectrum disorders. Brain Res 1309:83–94. [PubMed: 19896929]

Kaye WH, Wierenga CE, Bailer UF, Simmons AN, Bischoff-Grethe A (2013) Nothing tastes as good as skinny feels: the neurobiology of anorexia nervosa. Trends Neurosci 36:110–120. [PubMed: 23333342]

Keating C, Tilbrook AJ, Rossell SL, Enticott PG, Fitzgerald PB (2012) Reward processing in anorexia nervosa. Neuropsychologia 50:567–575. [PubMed: 22349445]

Kreple CJ, Lu Y, Taugher RJ, Schwager-Gutman AL, Du J, Stump M, Wang Y, Ghobbeh A, Fan R, Cosme CV, Sowers LP, Welsh MJ, Radley JJ, LaLumiere RT, Wemmie JA (2014) Acid-sensing ion channels contribute to synaptic transmission and inhibit cocaineevoked plasticity. Nat Neurosci 17:1083–1091. [PubMed: 24952644]

Luo J, Sladek R, Carrier J, Bader JA, Richard D, Giguere V (2003) Reduced fat mass in mice lacking orphan nuclear receptor estrogen-related receptor alpha. Mol Cell Biol 23:7947–7956. [PubMed: 14585956]

Lutter M, Croghan AE, Cui H (2015) Escaping the golden cage: animal models of eating disorders in the post-diagnostic and statistical manual era. Biol Psychiatry.

Oberlander JG, Woolley CS (2016) 17beta-estradiol acutely potentiates glutamatergic synaptic transmission in the hippocampus through distinct mechanisms in males and females. J Neurosci 36:2677–2690. [PubMed: 26937008]

Penzes P, Cahill ME, Jones KA, VanLeeuwen JE, Woolfrey KM (2011) Dendritic spine pathology in neuropsychiatric disorders. Nat Neurosci 14:285–293. [PubMed: 21346746]

Radley JJ, Rocher AB, Rodriguez A, Ehlenberger DB, Dammann M, McEwen BS, Morrison JH, Wearne SL, Hof PR (2008) Repeated stress alters dendritic spine morphology in the rat medial prefrontal cortex. J Comp Neurol 507:1141–1150. [PubMed: 18157834]

Roche KW, O'Brien RJ, Mammen AL, Bernhardt J, Huganir RL (1996) Characterization of multiple phosphorylation sites on the AMPA receptor GluR1 subunit. Neuron 16:1179–1188. [PubMed: 8663994]

Rodriguez A, Ehlenberger DB, Hof PR, Wearne SL (2006) Rayburst sampling, an algorithm for automated three-dimensional shape analysis from laser scanning microscopy images. Nat Protoc 1:2152–2161. [PubMed: 17487207]

Sala C, Segal M (2014) Dendritic spines: the locus of structural and functional plasticity. Physiol Rev 94:141–188. [PubMed: 24382885]

Salgado S, Kaplitt MG (2015) The nucleus accumbens: a comprehensive review. Stereotact Funct Neurosurg 93:75–93. [PubMed: 25720819]

Smink FR, van Hoeken D, Hoek HW (2012) Epidemiology of eating disorders: incidence, prevalence and mortality rates. Curr Psychiatry Rep 14:406–414. [PubMed: 22644309]

Stein RA, Chang CY, Kazmin DA, Way J, Schroeder T, Wergin M, Dewhirst MW, McDonnell DP (2008) Estrogen-related receptor alpha is critical for the growth of estrogen receptor-negative breast cancer. Cancer Res 68:8805–8812. [PubMed: 18974123]

Wagner A, Aizenstein H, Mazurkewicz L, Fudge J, Frank GK, Putnam K, Bailer UF, Fischer L, Kaye WH (2008) Altered insula response to taste stimuli in individuals recovered from restricting-type anorexia nervosa. Neuropsychopharmacology 33:513–523. [PubMed: 17487228]

Wang JQ, Arora A, Yang L, Parelkar NK, Zhang G, Liu X, Choe ES, Mao L (2005) Phosphorylation of AMPA receptors: mechanisms and synaptic plasticity. Mol Neurobiol 32:237–249. [PubMed: 16385140]

Wierenga CE, Bischoff-Grethe A, Melrose AJ, Irvine Z, Torres L, Bailer UF, Simmons A, Fudge JL, McClure SM, Ely A, Kaye WH (2015) Hunger does not motivate reward in women remitted from anorexia nervosa. Biol Psychiatry 77:642–652. [PubMed: 25481622]

Wojcik SM, Brose N (2007) Regulation of membrane fusion in synaptic excitation-secretion coupling: speed and accuracy matter. Neuron 55:11–24. [PubMed: 17610814]

Wu XS, Xue L, Mohan R, Paradiso K, Gillis KD, Wu LG (2007) The origin of quantal size variation: vesicular glutamate concentration plays a significant role. J Neurosci 27:3046–3056. [PubMed: 17360928]

Yang N, Shigeta H, Shi H, Teng CT (1996) Estrogen-related receptor, hERR1, modulates estrogen receptor-mediated response of human lactoferrin gene promoter. J Biol Chem 271:5795–5804. [PubMed: 8621448]

Zastrow A, Kaiser S, Stippich C, Walther S, Herzog W, Tchanturia K, Belger A, Weisbrod M, Treasure J, Friederich HC (2009) Neural correlates of impaired cognitive-behavioral flexibility in anorexia nervosa. Am J Psychiatry 166:608–616. [PubMed: 19223435]

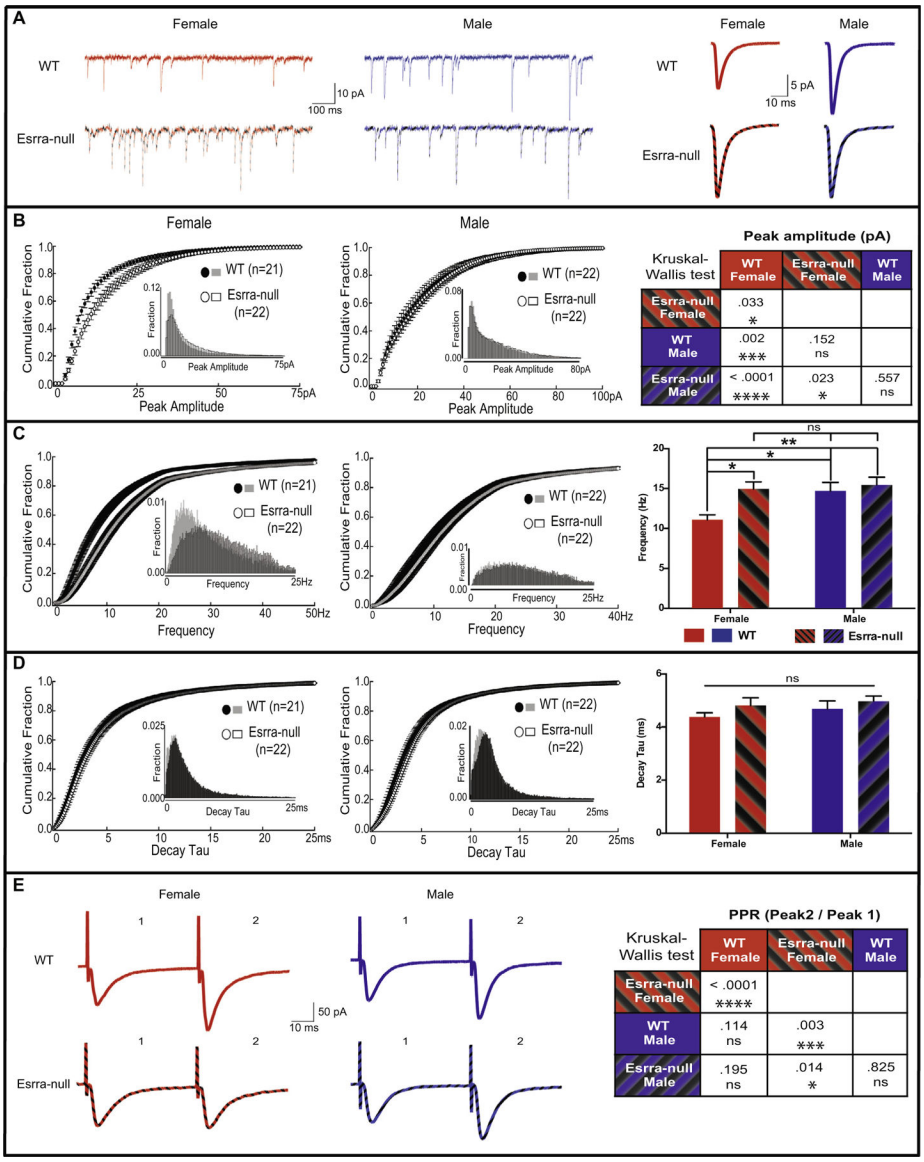

Fig. 1.

Altered synaptic physiology in female Esrra-null mice. (A) Sample traces of mEPSCs in the NAc core of both female and male WT and Esrra-null mice of individual recordings (left) and an average of all mEPSC events (right). Cumulative fraction and histogram (insets) distribution of mEPSC show an increased amplitude (B) and frequency (C), but not decay tau (D), in female Esrra-null mice. (E) Example traces of paired pulse ratio in the NAc core of female and male WT and Esrra-null mice showing a decrease in PPR only in female Esrra-null mice. Bar graphs are presented as mean ± S.E.M. Kruskal–Wallis was used to analyze non-normally distributed data (A, E) and two-way ANOVA for normally distributed data (C, D). *$p < .05$, **$p < .01$, ***$p < .001$, ****$p < .0001$ indicate significant differences between the groups.

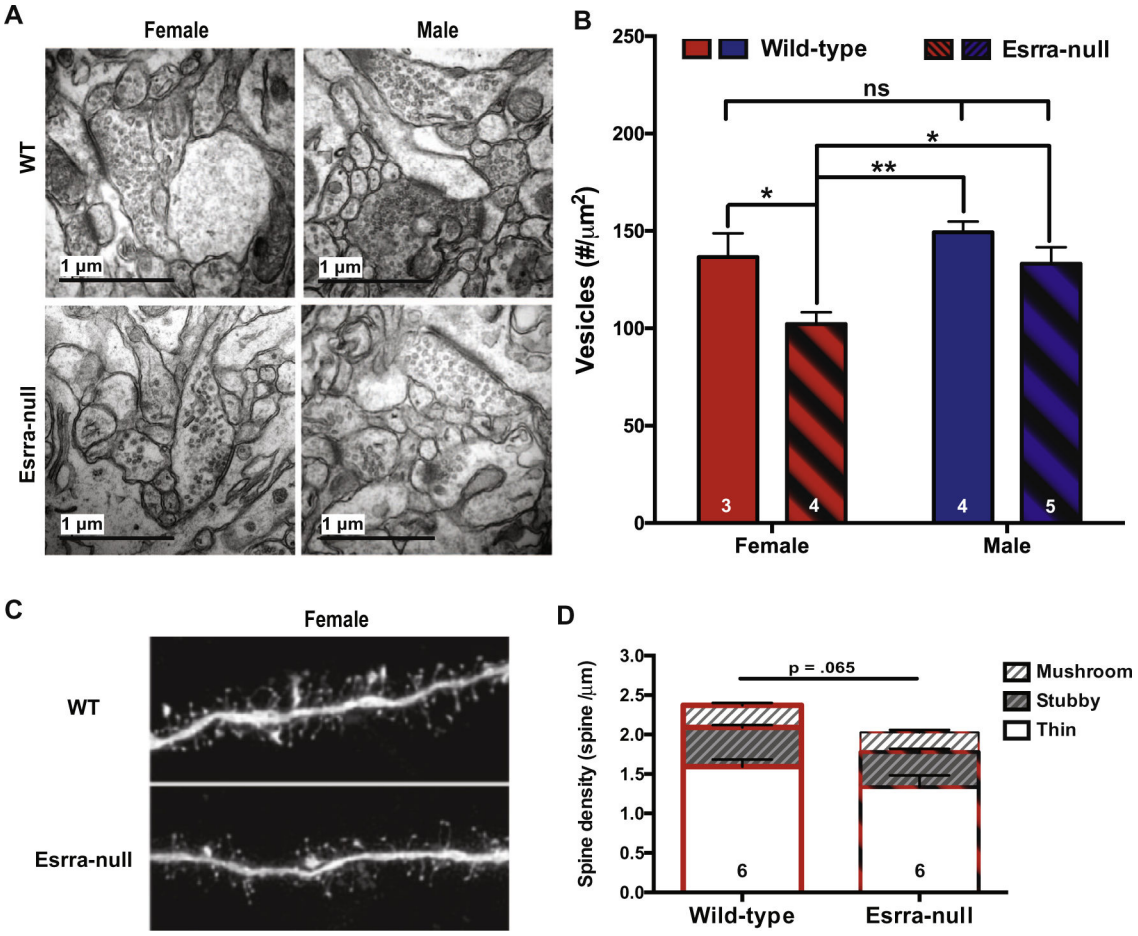

Fig. 2.

Decreased synaptic vesicle pool density in female Esrra-null mice. (A) Representative electron microscope images from NAc core of both females and male WT and Esrra-null mice. (B) Quantification of vesicle density from 34,535 vesicles in 508 synapses showing a significant reduction in females, but not male, Esrra-null mice. (C) Representative images of medium spiny neurons in the NAc core that were loaded with Lucifer yellow for dendritic spine density assessment in female WT and Esrra-null (KO) mice. (D) Quantification of 15,075 spines shows no statistically significant difference between female WT and Esrra-null mice. Data are presented as mean ± S.E.M. A two-way ANOVA was used in (B) and a Mann–Whitney *U* test was used for (D). $^{**}p < .01$, $^{***}p < .001$ indicate significant differences between the groups.

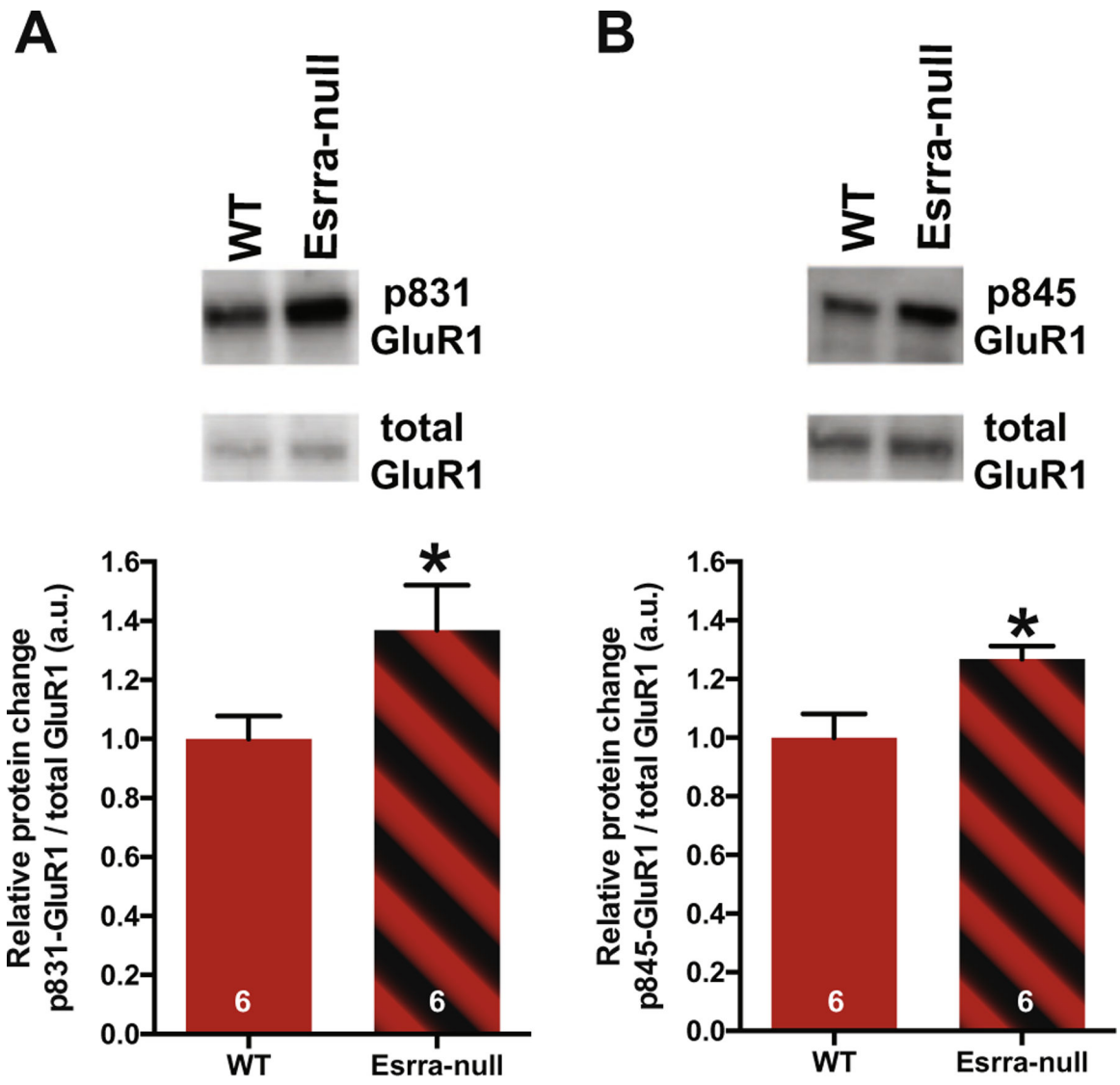

Fig. 3.

Increased levels of phosphorylation of GluR1 at Ser^{831} and Ser^{845} in nucleus accumbens of female Esrra-null mice. (A, B) Representative Western blot images of phosphorylated and total GluR1 in NAc (top) and densitometric analysis of phospho- to total GluR1 ratio in female WT and Esrra-null mice (bottom). Data presented as mean ± S.E.M. $*p < 0.05$ indicates significant differences between the groups (Mann–Whitney *U* test).